SUPPLEMENTRY MATERIAL

Immobilization of TBBPA on Freeze-Thaw-induced Pyrogenic Carbon with Natural Organic Matters: Insight into Surface Functionalization, Coverage Process and Bonding Affinity

Jian Shen[a], *Gordon Huang*[a,*], *Chunjiang An*[b], *Yao Yao*[a], *Xiaying Xin*[a], *Scott Rosendahl*[c]

[a] Institute for Energy, Environment and Sustainable Communities, University of Regina, Regina, Saskatchewan, Canada S4S 0A2

[b] Department of Building, Civil and Environmental Engineering, Concordia University, Montreal, Quebec, H3G 1M8, Canada

[c] Canadian Light Source, Saskatoon, Canada S7N 2V3

*corresponding author, phone: +1-306-585-4095; fax: 1-306-585-4855; e-mail: gordon.huang@regina.ca

Preparation of pyrogenic black carbons from pinecone biomass

Pinecone biomass was collected from Yellow pines (*Pinus. ponderosa*) from southern Saskatchewan, Canada. The procedure of preparing the pinecone-derived pyrogenic carbon was in accordance with standard method. Briefly, the collected pinecones were separated and washed with deionized water to remove impurities, and then air-dried for 2 days before being oven-dried at 110 °C for 24 h. After drying, the biomass samples were grounded and passed through a 0.425 mm standard sieve. Fine pinecone powder was tightly packed into a ceramic pot and covered with aluminum foil. The powder was pyrolyzed for 4 h at varying temperatures, such as high-temperature (550 °C) and low temperature (250 °C), in a muffle furnace in an oxygen-limited system. The heating rate was controlled at 5 °C /min. The pyrogenic carbon was then washed with pure water to neutral pH. The samples were further oven-dried 24 h at 85 °C.

Freeze-thaw aging process

The freeze-thaw treatment was performed a total 21 freeze-thaw cycles between cold condition (-20 °C) for 7 h and warm condition (30 °C) for 17 h. Given to the applied environment of the carbon materials and the need of freezing in physicochemical analysis, the freeze temperature and thaw temperature were set to -20 °C and 30 °C.

The pyrogenic black carbon through surface physical aging process during freeze-thaw method was labeled as FTBCP250 and FTBCP550.

The adsorption studies pyrogenic carbon surfaces with NOMs

To investigate the effects of different pyrogenic carbon surfaces on TBBPA adsorption, 10 mg of BCPs and FTBCPs were added into each glass vial with a certain initial TBBPA concentration. To investigate the effects of pH, different amounts of 0.01 M NaOH or HCl were added into each glass vial with initial TBBPA concentration ranging from 0.5 to 2 mg/L at temperature of 15, 25 and 35 °C. The adsorption experiments for TBBPA were conducted for all application rates of pyrogenic carbon. In kinetics experiments, TBBPA concentrations were monitored at different time points under temperature of 15, 25 and 35 °C. The interaction of NOMs with TBBPA adsorption on pyrogenic carbon surface was analyzed via adding certain humic acid sodium salt (10 ~ 30 mg/L) before the adding of TBBPA concentration.

The TBBPA stock solution was prepared in methanol and then diluted by the background solution containing 0.01 M CaCl2 and 200 mg/L NaN3 to simulate a constant ionic strength and inhibit microbial activity, respectively. It should be noted that methanol concentrations (methanol/water, v/v) were controlled at less than 0.1% to avoid co-solvent effects. The initial concentrations (0.5–2.0 mg/L) were determined to cover the range between detection limit and aqueous solubility. Blank controls (i.e.,

without sorbents) were run concurrently to investigate sorption to the glassware wall. The experiments were also conducted in the dark to prevent photolysis.

HPLC setting

An Agilent Infinity 1260 high-performance liquid chromatography system (USA) equipped with a ZORBAX XDB-C18 column and a diode array detector (DAD) operated at a wavelength of 210 nm was used to measure the concentration of TBBPA. A mobile phase consisting of methonal/water (85:15, v/v) was used at a flow rate of 0.7 mL/min, and the column temperature was set to 30 degrees. In this condition, the specific peak of TBBPA can be observed in 6 mins. The specific surface area of carbon materials was determined at 77 K with a TriStar II 3020(Micromeritics, USA). Zeta potential was measured with Anton Paar SurPASS™ 3 is a high-end electrokinetic analyzer.

The quality assurance and quality control

The quality assurance program was followed to ensure the accuracy and reliability of the collected data. All batch experiments were conducted in triplicate and average values were reported (relative standard deviation less than 5%). Blank tests were run and corrections were applied if necessary. All containers used in this study has been previously cleaned with the particular washing liquid for laboratory purposes, triply rinsed with distilled water and oven dried. Experimental runs have been performed by

using a TBBPA containing solution without addition of pyrogenic carbon. The corresponding results confirmed that the initial TBBPA concentration remained unchanged during the experiment. It indicated that the reduction of TBBPA concentration in experiments was only related to the adsorption on pyrogenic carbon samples.

Synchrotron-based SD-FTIR analysis on different pyrogenic carbons

The pyrogenic carbon surface from low-temperature pyrolysis exhibits different functional groups compared with that from high-temperature pyrolysis. Fig. S2 shows that BCP550 has strong responses at 3010 and 2970 cm-1, representing distinguishable aromatic groups of v(C=CH) and v(—C=CH2). Sharp peaks at 2960, 2925, 2870 and 2850 cm-1 indicate stable structure of alkanes. Compared to BCP250 which has multiple responses in the range of 3100 to 2800 cm-1, BCP550 contains high content of stable aromatics. Remarkable responses of 1450, 1500 and 1580 cm-1 showed in BCP550 suggest formidable aromatic cycles on the surface with stable branches of —CH3 (1390 and 1365 cm-1) and —CH2— (1400 cm-1). However, instead of five consequent responses of v(C—O—C) between 1100 and 1050 on BCP550, BCP250 exhibits strong response of hydroxyl groups in v(C—OH) at 1150 cm-1. Therefore, more active hydroxyl groups and more variety of oxygen-containing groups can be found on low-temperature pyrogenic carbon surface than high-temperature one.

Synchrotron-based SD-FTIR analysis on physical aged carbons

the notable differences are found between BCP250 and FTBCP250 (Fig.S2), indicating the changes of surface functionality after physical aging. The peak changes close to 1750, 1400, 1250, 1080, 1020 and 880 cm-1, indicates that alkene branches, aromatic structures and unsaturated oxygen-containing groups are affected, respectively. Strong responses of v(C=CH2) and v(C—H) at 890, 880 and 860 cm-1 are observed in FTBCP250. The strong peaks at 1400, 1380 and 1370 cm-1 for C—H bending of alkene represent that the surface of FTBCP250 has predominated aromatic structures. Although FTBCP250 also presents active hydroxyl groups of similar response at 1150 cm-1, the responses of functional groups in the range from 1300 to 1000 cm-1 are altered. After physical aging, specific weak oxygen containing groups related to stable aromatic structures are enhanced while most of oxygen containing groups are decreased, resulting in the decrease of variety in functional groups. The medium response at 1050 cm-1 on BCP250 splits into two very strong responses at 1060 and 1040 cm-1 in FTBCP250, indicating the changes in symmetry of surface complexes.[1] Therefore, as shown in Fig. 3, from the view of surface functionality, a "homo-functionalization" process can be used to describe the surface structure development in physical aging process through the consolidation of oxygen containing groups with aromatic structures and antagonization of other active hydroxyl groups.

The effect of contact time on adsorption of TBBPA

The overall contact process can be divided into two major stages. In the early stage, a rapidly uptake of TBBPA is observed on the surface. The following stage exhibits a gradual increase of TBBPA removal, and the removal is approaching an uptake limit of pyrogenic carbon surface eventually. As the contact process and uptake curve can be found similar with adsorption process [2], the surface interaction between TBBPA and pyrogenic carbon surface can be predominated as adsorption process.

Adsorption kinetic analysis for surface estimation

The Lagergren pseudo-first order kinetics model, is expressed as:

$$Q_t = Q_e(1 - e^{-k_1 t}) \qquad (1)$$

where Q_t (mg/g) represents the amount of adsorbate adsorbed at a predetermined time, t (min) and Q_e (mg/g) is the amount of adsorbate adsorbed at equilibrium and k_1 (1/min) is the rate constant.

The Lagergren pseudo-second order kinetics model is defined as:

$$Q_t = \frac{Q_e^2 k_2 t}{1 + Q_e k_2 t} \quad \text{and} \quad h = k_2 Q_e^2 \qquad (2)$$

where k_2 (g/mg min) is the pseudo-second order rate constant and h (mg/g min) is the initial adsorption rate.

Intra-particle diffusion rate model helps determine the rate-controlling step as that of

pore diffusion in an adsorption mechanism and described as:

$$Q_t = k_p t^{0.5} + C \quad (3)$$

where k_p (mg/g min$^{0.5}$) is the intra-particle diffusion rate constant and C (mg/g) is a constant that describes the boundary layer effect. Higher C values are indicative of higher boundary layer effect and thus are descriptive of the inapplicability of pore diffusion as the sole rate-determining step in describing the dynamics of the adsorption process.[3] If C = 0, the adsorption kinetics are controlled only by intraparticle diffusion. If $C \neq 0$, the adsorption process is quite complex.[4]

Elovich model involves the chemisorption in solid surface, and the decrease of adsorption velocity due to the covering of superficial layer, [5] which can be described as:

$$Q_t = \frac{1}{\beta} log_e(\alpha\beta) + \frac{1}{\beta} log_e(t) \quad (4)$$

where the α is the initial adsorption rate (g/(mg min)), and the β is desorption constant (g/mg). [6, 7]

Thermodynamic calculations and estimations

Thermodynamic parameters were calculated using following equations:

$$\ln K = \frac{\Delta S^{\circ}}{R} - \frac{\Delta H^{\circ}}{RT} = -\frac{\Delta G^{\circ}}{RT} \quad (5)$$

$$K_c = \frac{C_e}{C_s} \quad (6)$$

where T(K) is the temperature of solution, K_c is the adsorption equilibrium content, R is the gas constant. Enthalpy (ΔH°) and entropy (ΔS°)were calculated via slope and intercept from Van't Hoff plot of $\ln K$ versus $1/T$ where the K value can be derived from equilibrium concentrations (K_c), Langmuir isotherms (K_L) and Freundlich isotherms (K_F). Gibbs free energy (ΔG°) was calculated based on $\ln K$ of different derives.[8]

3.4 Kinetics for the adsorption of TBBPA on pyrogenic carbon

Adsorption kinetics study can help explore the adsorption mechanism. The kinetic models including the pseudo-first-order, pseudo-second-order and intraparticle diffusion models, were used in this study (see Supporting Information).

Uptake on carbon surfaces in water solution. Fig. 3 and Table.S1 shows that pseudo-first order, pseudo-second order and Elovich models can fit the experiment data with the correlation coefficients (R^2) higher than 0.90. The poor fitting of intra-particle model indicates that the behavior of TBBPA on carbon surfaces is not predominantly affected by either instantaneous external surface adsorption or gradual intra-particle diffusion, and the rate-limiting step in the adsorption is not intra-particle diffusion. [34, 35] Moreover, as the pseudo-first order model has lower R^2 than pseudo-second order model, the chemisorption can be the limiting step for TBBPA

adsorption on carbon surfaces.[35] It indicates the interaction of functional groups can determine the adsorption rate of TBBPA. In addition, Elovich model also shows relatively good fitting, suggesting the chemisorption of TBBPA on the solid carbon surface.

Uptake on carbon surface with NOMs. Fig. 3 (e ~ l) shows the significantly different uptakes of TBBPA under instant and constant contact of NOMs with carbon surfaces. The better fitting in Table. S1 indicates intra-particle diffusion frequently happens with constant NOMs involved. The result also suggests that the low-pyrogenic carbon surfaces can be more possible to be covered by NOMs layers during constant than instant contact conditions. In contrast, the high-pyrogenic carbon surface (FTBCP550) with physical aging process exhibits much lower R^2. For the adsorption on, FTBCP550, the pseudo-first order and pseudo-second order models exhibits better performance with instant contact, while lower R^2 for pseudo-first order and improved R^2 for intra-particle diffusion model is observed for constant condition. It The adsorption processes under such iInstant and constant conditions are different. Moreover, the distinguishable decrease of R^2 of pseudo-first order model for instant conditions with BCP250 indicates more factors are involved in the adsorption process.

The different adsorption behaviors on BCP250 and FTBCP550 under these conditions can be attributed to the change of surface properties and corresponding NOMs effects. Based on the discussion above, the adsorption process of TBBPA on carbon surface with NOMs is depicted in Fig.5. The surface functionality may favor the adsorption of NOMs,[36] and TBBPA in NOMs solution can form TBBPA-HA, BCP-HA and BCP-TBBPA interactions.[13, 33] High functionality carbon surface produced from low pyrolysis temperature can have more active sites for NOMs than low functionality

carbon surface from high pyrolysis temperature. With constant contact with carbon surfaces, there would be more coverage of NOMs on BCP250 than BCP550. The carbon surface covered with NOMs may also adsorb TBBPA to form TBBPA-HA-BCP linkage. However, as the free TBBPA-HA is hard to be abstracted, the adsorption of TBBPA on NOMs surface cannot compensate that on original pyrogenic carbon surface, leading to a decline in adsorption rate. Under instant contact with simultaneous addition of TBBPA and NOMs, however, there is a radical competing adsorption between NOMs and TBBPA. Moreover, unlike the surface covered with NOMs, large number of TBBPA-HA can be formed and hard to attach to the active sites of carbon surface. That could result in the lower adsorption rate under NOMs instant contact than that under constant contact. Furthermore, since the high-pyrogenic carbon surface has inactive functional groups for NOMs and TBBPA adsorption, both contact processes showed similar negative effects on TBBPA adsorption. The surface tension can decrease in the presence of NOMs [37] and the porous adsorption enhanced from physical aging process can be blocked in NOMs solutions. Thus, FTBCPs have similar or worse adsorption performance compared with BCPs.

Adsorption of TBBPA concentrations on pyrogenic carbon surfaces at different environmental temperatures

Fig. 4 shows that various pyrogenic carbon surfaces expressed different adsorption patterns as temperature changed. It not only shows that the carbon surfaces from lower pyrolysis temperature have better removal of TBBPA, but also indicates that pyrolysis processes can have more substantial influence on TBBPA adsorption than

physical aging. Furthermore, although the difference between adsorption patterns of BCP250 and FTBCP250 is not obvious in most environmental temperatures, the TBBPA adsorption on FTBCP550 is significantly higher than that on BCP550. The results suggest that the physical aging process can improve the TBBPA uptake on carbon surface. Given that there is no tremendous change upon adsorption trends, the physical aging process may not able to severely alter the surface properties of pyrogenic carbon.

The presence of humic acids showed significant impact on the adsorption of TBBPA. With the addition of adding 10 mg/L humic acids, the adsorption slightly decreased on BCP250 and corresponding physical aged surface. The adsorption on BCP550 and corresponding physical aged surface greatly decreased after the addition of humic acids, while the difference between original carbon surface and physical aged surface is reduced. Similar narrowing trend for adsorption was also observed on BCP250, BCP550 and their physical aged surfaces. The different adsorption behaviors may be attributed to specific surface impacted by both pyrolysis temperature and physical aging process. There would be enhanced adsorption due to the increasing porosity of carbon surface after physical aging. When the humic acids were added, they can initially interfere with physical adsorption. When large amount of humic acids presents, humic acids can start to compete with function groups on the surface, causing suppressed surface interactions on BCP250 and FTBCP250. Therefore, the humic acids can affect both physical adsorption and function group interaction with TBBPA on carbon surface.

3.6 Adsorption isotherms analysis in different temperatures

The equilibrium retention of TBBPA onto pyrogenic carbon with different surface properties can be mathematically described via numerical models with physical-chemical assumption and empirical inference. Types of surface coverage including homogeneity and heterogeneity were considered in those models. The surface interactions between TBBPA and function groups were further explored using adsorption isotherm modeling. Langmuir, Freundlich and Langmuir-Freundlich isotherm models were used in this study(Supporting Information).[38] The adsorption isotherms and calculated results are shown in Fig. S3, Table S2 and Table. S3, respectively. The Langmuir isotherm can be expressed as follow:

$$Q_e = \frac{q_m K_L C_e}{1+K_L C_e} \quad (5)$$

where q_e (mg/g) and C_e (mg/L) are the amount of sorbed TBBPA per unit mass of adsorbent and TBBPA concentration at equilibrium, respectively. q_m (mg/g) is the maximum amount of the TBBPA per unit mass of adsorbent to form a complete monolayer on the surface. K_L is a constant related to the affinity of the binding sites (L/mg).

The Freundlich isotherm model, an empirical equation, is used to describe heterogeneous surfaces [25]. The Freundlich equation is:

$$Q_e = K_F C_e^{\frac{1}{n}} \quad (6)$$

where K_F is an empirical constant related to the sorption capacity of the adsorbent (L mg^{-1}) and constant n is an empirical parameter related to the intensity of sorption and varies with surface heterogeneity and affinity. The value of n gives an indication of the favorability of the sorption.

The Langmuir-Freundlich isotherm model [26] is:

$$Q_e = \frac{q_{m^*} b {C_e}^{n^*}}{1 + b {C_e}^{n^*}} \quad (7)$$

b is the adsorption equilibrium constant relating to the binding energy of the adsorption system. n^* is indicative of the surface site heterogeneity of the adsorbent.

Fig. 4 shows the adsorption patterns on varied carbon surfaces are different. When the environmental temperature increased from 288 K to 308 K, the uptake of TBBPA generally decreased. It indicates the adsorption is an exothermic process for various pyrolysis and physical aging conditions. Such exothermic feature for TBBPA adsorption was also found on other carbon materials such as graphene oxide[33] and carbon nanotube.[39] Additionally, the involvement of NOMs can have significant impact on adsorption under different environmental temperatures. That suggests NOMs can result in unneglectable thermodynamic changes in the interaction between TBBPA and carbon surfaces. With the increased amount of NOMs, the uptake of TBBPA on carbon surfaces is decreased and the interaction is changed to the endothermic process.

When Freundlich model presents good fitting, it indicates a multilayer adsorption is

involved between adsorbed TBBPA and carbon surfaces.[40] The n values higher than 1 suggest the adsorption is favorable and the active sites on the carbon surface for TBBPA are heterogeneous for TBBPA adsorption. Nevertheless, as the relatively high R^2 of Langmuir model is approached, the adsorption can be more suitable to be described as the formation of monolayer coverage on the carbon surface. When the R_L value is below than 1, the adsorption of TBBPA on carbon surface could be favorable. Q_m significantly decreases with the involvement of NOMs, suggesting NOMs can cause great negative impact on TBBPA adsorption. Moreover, the Langmuir-Freundlich isotherm model showed a better overall fitting than Langmuir and Freundlich isotherm models. It indicates both heterogenetic and monolayer adsorption can be involved. The deviation of n^* value from 1 shows that the multilayer adsorption could take place for attracting TBBPA to the active sites on heterogenous surface.

n values from Freundlich isotherm model for BCP250 and BCP550 in non-NOMs solution increase for FTBCP250 and FTBCP550 after physical aging. It indicates that the physical aging process can result in more active sites on the extended heterogenous carbon surfaces for TBBPA adsorption. However, n^* from Langmuir-Freundlich model drops down after physical aging process. It can be attributed to the increasing surface area and surface complexity, which enhances physical adsorption on porous surface rather than attraction to the active sites. Additionally, after adding NOMs, an increase in n value is observed on most carbon surfaces. It can be explained that the involvement of NOMs can enhance the multilayer adsorption because NOMs could capture and replace the active sites on the heterogenous surface and compete with TBBPA. The n^* values slightly increase

after adding NOMs. It suggests that physical adsorption can be reduced due to the decrease of surface tension. As most pores are filled with NOMs, the active sites struggle to attract TBBPA to the carbon surface from NOMs solution.

Thermodynamic analysis of NOMs competing adsorption

The changes in thermal performances and thermodynamic characteristics of adsorption reflects the impacts of NOMs solutions (Table S4). The adsorption of TBBPA on carbon surface competed with NOMs in the solution, resulting the highest TBBPA adsorption at 298 K compared to the adsorption at 288 and 303 K in the presence of 10 mg/L of NOMs. It can be explained that during the competition with NOMs, the system also had some endothermic NOMs-TBBPA interactions, such as solubilization and surface activity effects. The endothermic reactions can thus compete with exothermic reactions at different temperatures, resulting in inconsistent thermodynamic behavior of TBBPA on carbon surface. Additionally, in both 10 and 30 mg/L NOMs solutions, ΔS° exhibited positive values, indicating TBBPA in the system was partially dispersed. The positive ΔH° values showed that external energy was needed for TBBPA uptake and partial TBBPA might need external energies to be subtracted from NOMs solutions. Moreover, the calculated thermodynamic parameters based on K_c and K_F indicated that, as the ΔG° showed negative value, the adsorption was still carried out spontaneously, even the thermal performance switched from exothermic to endothermic reactions.

Site distribution discussions of in NOMs interactions

$\mu(E^*)$ and σ_e^* show different values under different NOMs solutions and

temperature conditions. That suggests the affinity, interaction strength and heterogeneity of carbon surface can be affected by NOMs and environmental temperature. In the solutions without NOMs, $\mu(E^*)$ generally decreased as temperature changed from 288 to 308 K.

In 10 mg/L NOMs solutions, the adsorption of TBBPA was significantly interfered with the competition effects of carbon surface and NOMs. Different carbon surfaces show increased and dissimilar interaction strength under changing temperatures. The carbon surface may compete to adsorb both TBBPA and NOMs, resulting in partial NOMs coverage on carbon surface with TBBPA-carbon surface and TBBPA-NOMs interactions. In 30 mg/L NOMs solutions, the carbon surface is covered by NOMs and the interaction of TBBPA-NOMs-carbon surface play a major role in TBBPA adsorption. Similar to the inverse thermodynamic behavior trend caused by NOMs, $\mu(E^*)$ decreased as temperature changed from 308 to 288 K. It could further reveal that the interaction strength and affinity in the adsorption can be significantly affected with the involvement of NOMs.

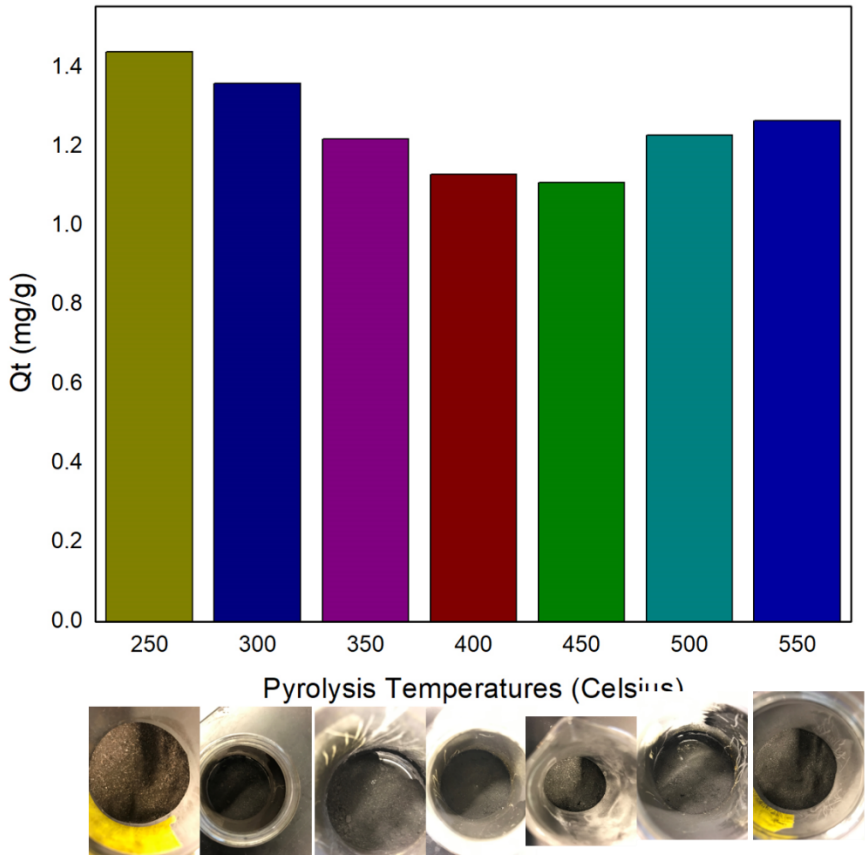

Fig.S1 Removal rate of Pyrolysis temperature from 250~550 ℃

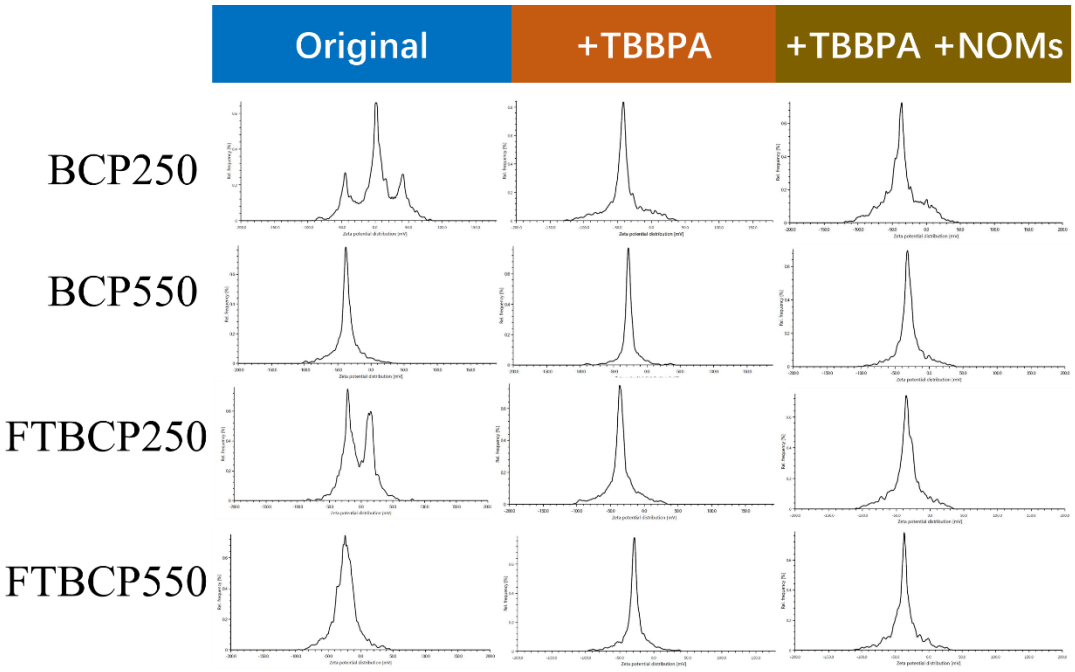

Fig. S2. Zeta potential results of different pyrogenic carbons

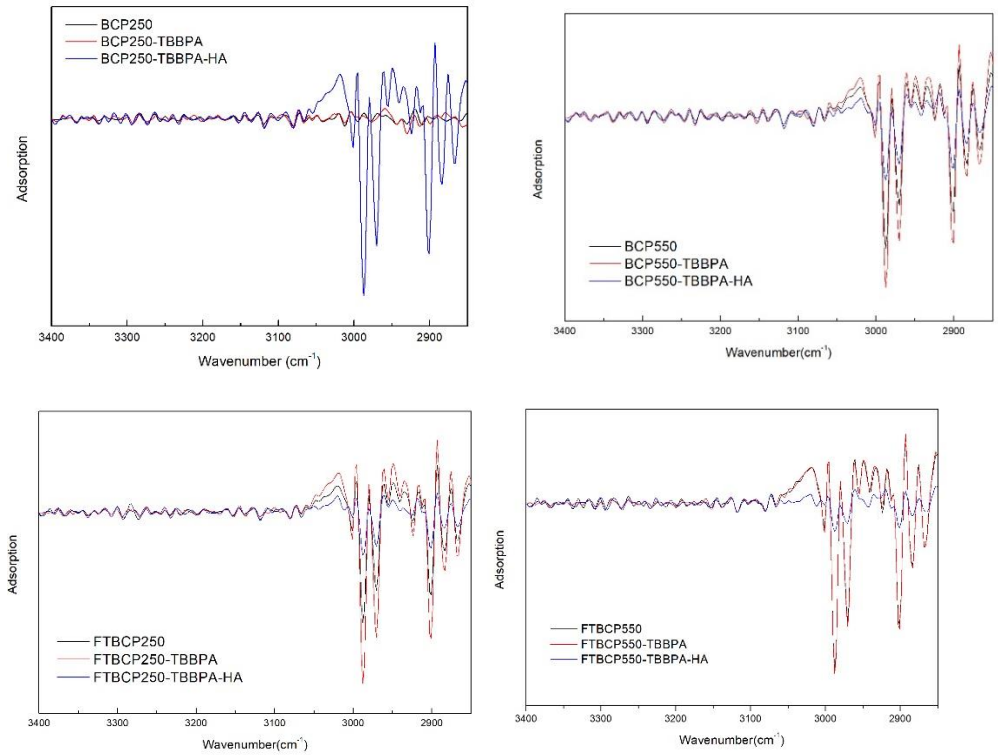

Fig S3 SR-SD-FTIR analysis on 3400-2900 cm-1

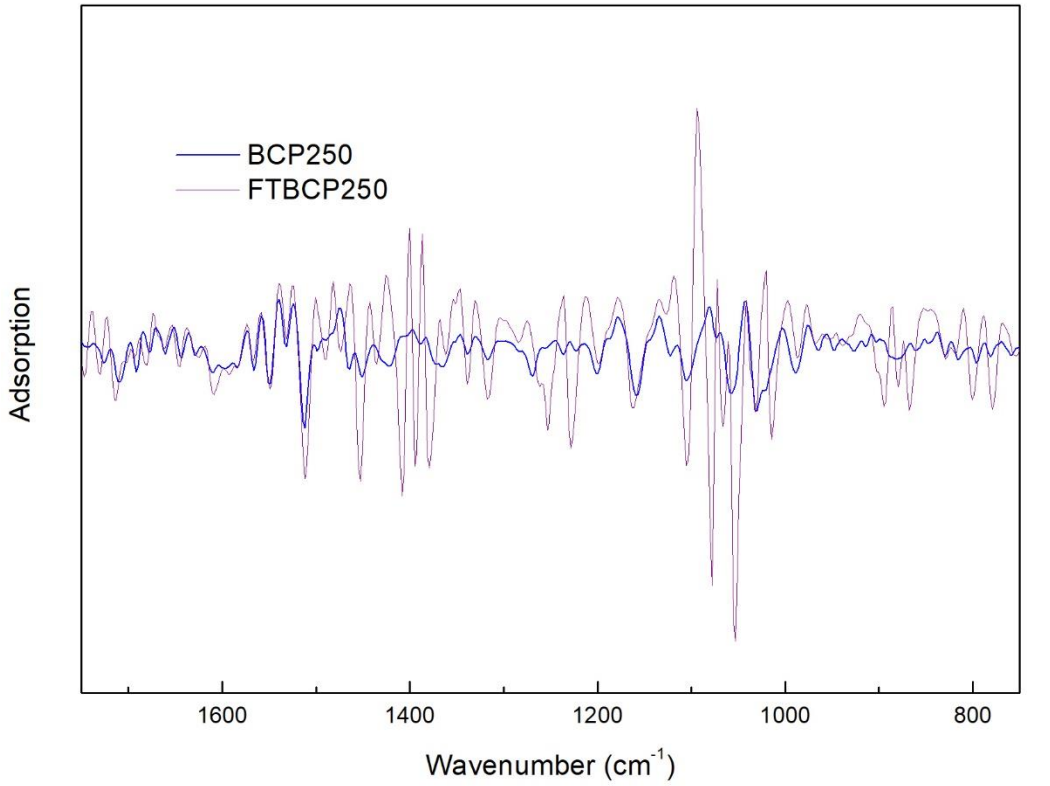

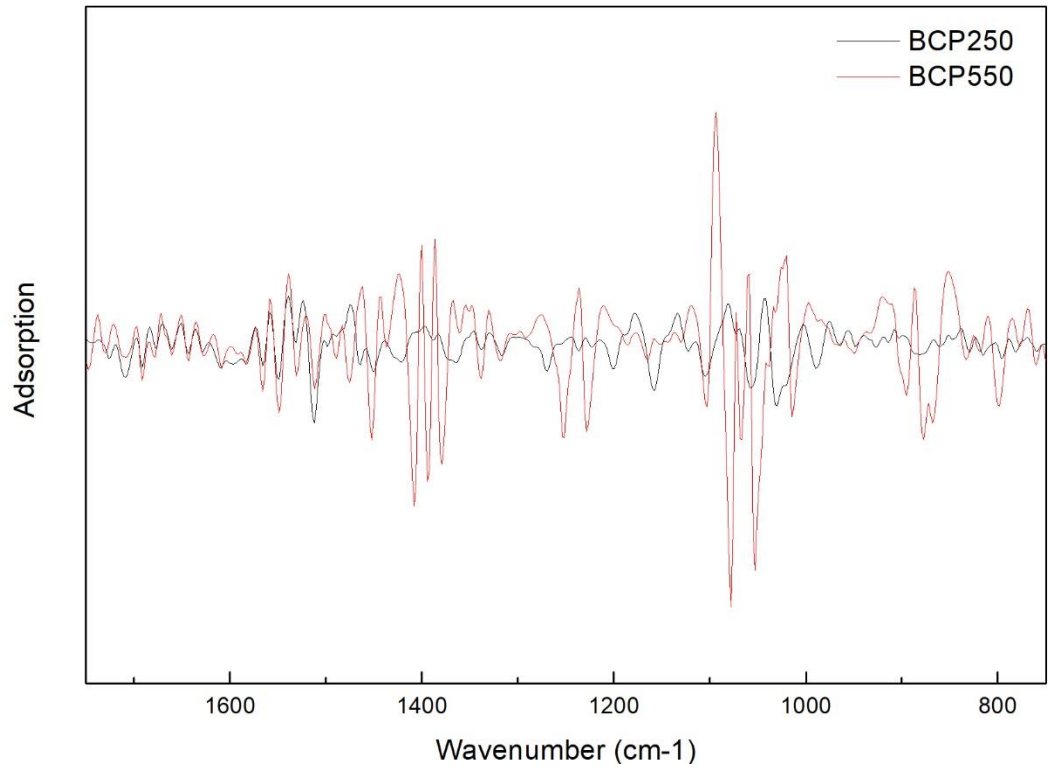

Fig.S4. Changes from pyrolysis and physical aging process

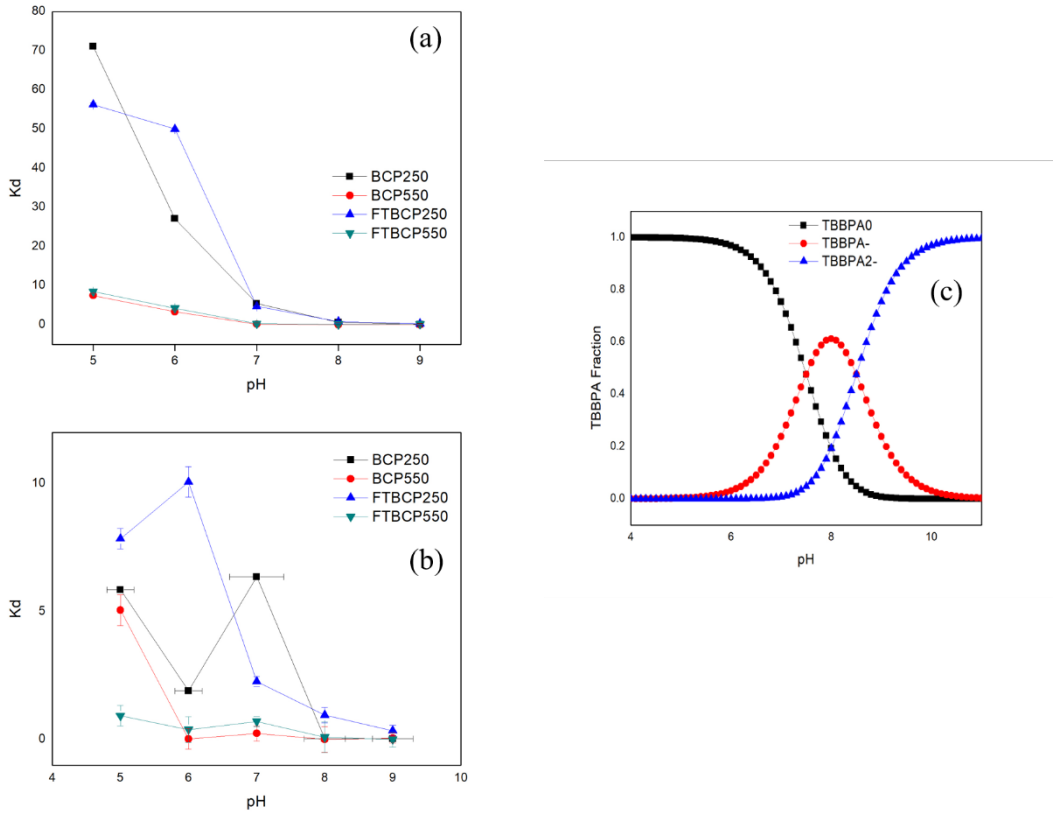

Fig. S5. Partition coefficient changes with pH and NOMs, (a) 1 mg/L TBBPA, (b) 1mg/L TBBPA and 30 mg/L NOMs, (c) Distribution of TBBPA dissociation fraction

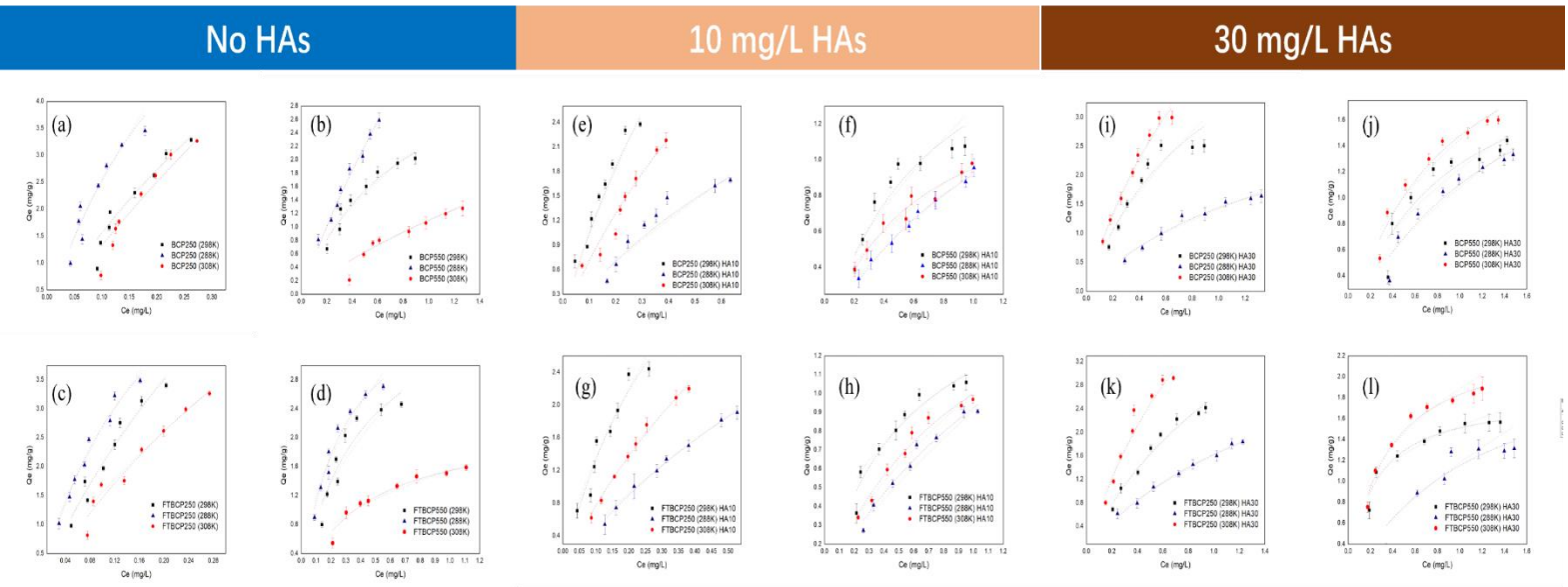

Fig.S6. Fitted adsorption data with Langmuir model (purple dash line) and Freundlich model (yellow dot line) for (a) BCP250, (b) BCP550, (c) FTBCP250, and (d) FTBCP550 in water, (e) BCP250, (f) BCP550, (g) FTBCP250, and (h) FTBCP550 in 10 mg/L HAs, (i) BCP250, (j) BCP550, (k) FTBCP250, and (l) FTBCP550 in 30 mg/L HAs.

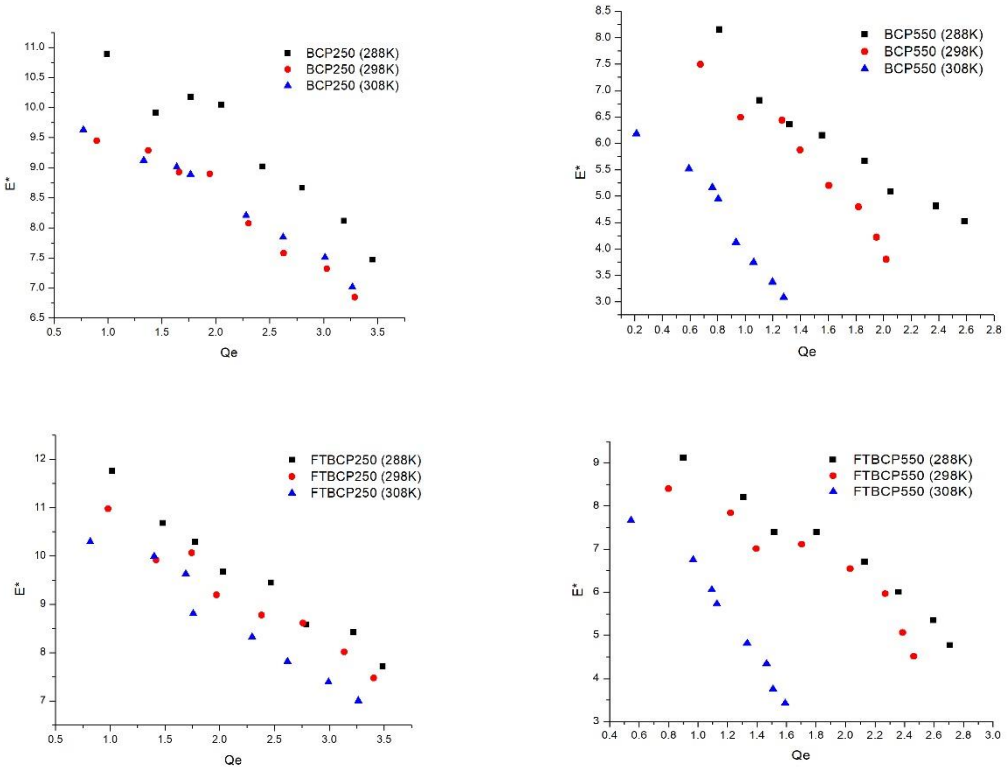

Fig. S7 Site energy changes with environmental temperatures on different pyrogenic carbon surfaces

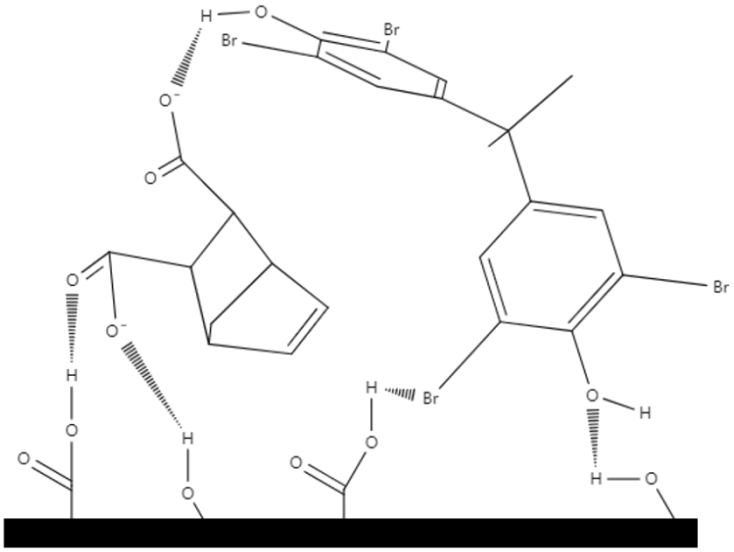

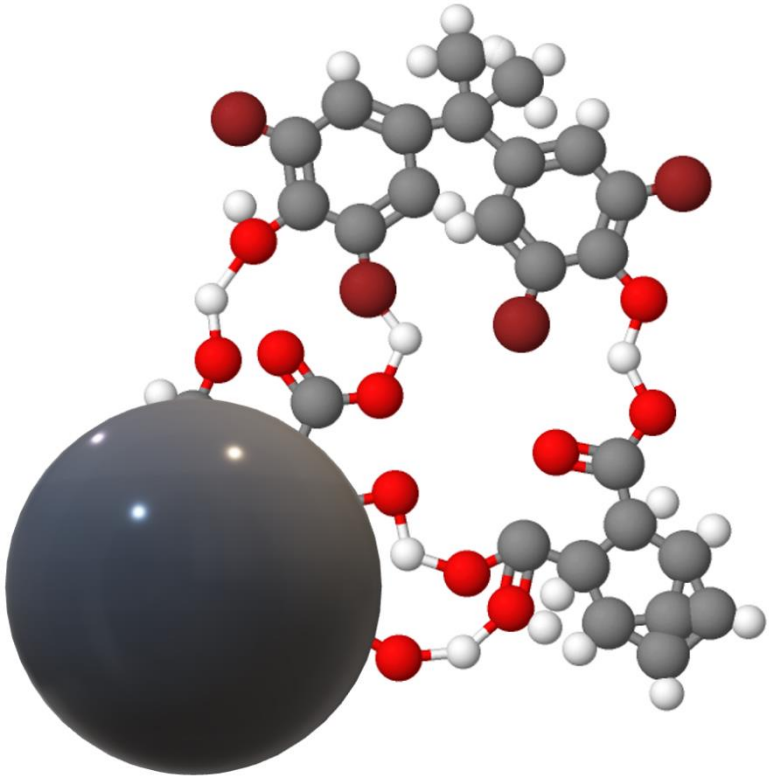

Fig. S8 Approached hydroxyl interactions under NOMs solutions

	N_{ad} (%)	C_{ad} (%)	H (%)	$S_{t, ad}$ (%)	O (%)	H/C	O/C	BET	(O+N)/C
BCP250	0.70	55.80	5.14	0.22	38.14	0.09	0.68	2.61	0.70
BCP550	0.90	70.70	2.52	0.11	25.77	0.04	0.36	10.00	0.38
FTBCP250	0.85	52.19	4.89	0.18	41.89	0.09	0.80	2.95	0.82
FTBCP550	0.87	72.92	2.64	0.07	23.50	0.04	0.32	19.64	0.33

Table S1. Results of Elemental analysis and BET surface analysis

Table S2. Calculated kinetics parameters of TBBPA adsorption under different contact scenarios.

Scenarios	Adsorbent	Pseudo-first-order			Pseudo-second-order				Intra-particle model			Elovich model		
		$Q_{e\ cal}$/(mg/g)	k_1 (L/min)	R^2	$Q_{e\ cal}$/(mg/g)	k_2 (g/mg min)	h	R^2	k_p (g/mg $min^{0.5}$)	C	R^2	α (g/mg min)	β (g/mg)	R^2
Standard	BCP250	1.851	0.075	0.951	1.930	0.065	0.239	0.987	0.031	1.101	0.428	54.759	6.373	0.957
	BCP550	0.803	0.082	0.952	0.827	0.194	0.278	0.964	0.011	0.516	0.289	20.465	8.604	0.917
	FTBCP250	1.913	0.069	0.946	1.995	0.058	0.231	0.989	0.034	1.108	0.464	31.043	5.838	0.967
	FTBCP550	1.723	0.066	0.986	1.797	0.060	0.181	0.985	0.030	0.996	0.416	22.934	6.401	0.914
Interference	BCP250	1.658	0.077	0.797	1.757	0.061	0.251	0.869	0.037	0.862	0.664	6.192	5.581	0.958
	BCP550	0.871	0.087	0.980	0.897	0.188	0.136	0.974	0.012	0.569	0.267	13.683	12.618	0.883
	FTBCP250	1.536	0.107	0.888	1.603	0.111	0.293	0.945	0.026	0.953	0.440	7.426	6.110	0.951
	FTBCP550	0.916	0.135	0.958	0.938	0.332	0.325	0.973	0.012	0.633	0.261	14.587	11.636	0.887
Intruding	BCP250	1.847	0.021	0.869	1.981	0.016	0.064	0.950	0.631	0.048	0.802	6.336	5.720	0.885
	BCP550	0.803	0.082	0.952	0.827	0.194	0.118	0.964	0.011	0.516	0.289	16.739	14.139	0.898
	FTBCP250	1.620	0.063	0.952	1.698	0.059	0.154	0.985	0.029	0.913	0.461	11.649	6.360	0.942
	FTBCP550	0.839	0.106	0.629	0.863	0.253	0.182	0.841	0.006	0.698	0.509	30.858	14.009	0.592

Table S3. Calculated parameters of isotherm models for TBBPA adsorption under different NOMs solution

Humic Acid	Adsorbent	Temperature (K)	Langmuir				Freundlich		
			Q_m (mg/g)	K_L (L/mg)	R_L	R^2	1/n	K_F (mg/g)	R^2
No HAs	BCP250	288	9.350	3.740	0.118	0.947	1.337	14.020	0.930
		298	11.201	1.616	0.236	0.858	1.253	9.824	0.849
		308	21.576	0.658	0.432	0.963	1.112	10.562	0.960
	BCP550	288	11.634	0.470	0.515	0.975	1.176	3.986	0.975
		298	3.960	1.276	0.282	0.939	1.600	2.313	0.909
		308	4.436	0.330	0.602	0.859	1.232	1.100	0.847
	FTBCP250	288	7.637	5.462	0.084	0.974	1.466	12.701	0.960
		298	11.810	2.106	0.192	0.980	1.241	12.982	0.943
		308	11.899	1.405	0.262	0.948	1.333	8.754	0.955
	FTBCP550	288	4.263	3.519	0.124	0.960	1.957	3.910	0.920
		298	4.174	2.516	0.166	0.865	1.828	3.310	0.814
		308	2.228	2.259	0.181	0.959	2.336	1.549	0.916
10 mg/L HAs	BCP250	288	5.305	0.765	0.395	0.938	1.250	2.519	0.923
		298	8.284	1.441	0.258	0.963	1.236	6.710	0.953
		308	7.450	1.047	0.323	0.952	1.261	4.589	0.964
	BCP550	288	2.026	0.826	0.377	0.986	1.513	0.927	0.988
		298	2.073	1.432	0.259	0.895	1.618	1.286	0.837
		308	1.503	1.720	0.225	0.964	1.898	0.973	0.952
	FTBCP250	288	6.338	0.827	0.377	0.994	1.300	3.189	0.986
		298	6.039	2.821	0.151	0.928	1.445	6.701	0.884
		308	7.161	1.199	0.294	0.992	1.259	4.899	0.984
	FTBCP550	288	2.583	0.557	0.473	0.970	1.263	0.909	0.967
		298	1.743	1.792	0.218	0.930	2.123	1.139	0.908
		308	2.041	0.959	0.343	0.968	1.431	1.009	0.976
30 mg/L HAs	BCP250	288	3.510	0.697	0.418	0.971	1.504	1.423	0.952
		298	5.647	1.138	0.305	0.912	1.466	3.211	0.864
		308	8.277	0.968	0.341	0.977	1.297	4.563	0.982
	BCP550	288	2.699	0.692	0.419	0.926	1.555	1.801	0.898
		298	2.331	1.177	0.298	0.844	1.838	1.222	0.787
		308	2.724	1.185	0.297	0.930	1.923	1.447	0.904
	FTBCP250	288	4.272	0.614	0.449	0.993	1.445	1.615	0.992
		298	6.178	0.719	0.410	0.967	1.408	2.649	0.953
		308	8.271	0.853	0.370	0.970	1.350	4.176	0.928
	FTBCP550	288	2.389	0.930	0.350	0.889	1.527	1.176	0.833
		298	1.818	4.922	0.092	0.932	3.571	1.529	0.880
		308	2.394	3.245	0.134	0.973	2.688	1.886	0.911

Table S4 Parameters from adsorption model of Langmuir-Freundlich model

Humic Acid	Biochar	Temperature (K)	Langmuir-Freundlich			
			b_* (L/mg)	q_{m*} (mg/g)	n*	R^2
No Humic Acid	BCP250	288	4.248	108.884	1.817	0.959
		298	3.774	151.960	2.435	0.937
		308	3.845	192.120	2.724	0.987
	BCP550	288	6.504	1.106	2.100	0.975
		298	2.274	10.210	1.993	0.963
		308	1.265	8.346	3.359	0.935
	FTBCP250	288	4.699	42.692	1.468	0.971
		298	5.242	21.719	1.513	0.955
		308	6.060	6.235	1.295	0.941
	FTBCP550	288	3.145	16.946	1.566	0.973
		298	2.599	60.265	2.491	0.939
		308	1.684	9.995	1.861	0.971
10 mg/L	BCP250	288	1.813	43.839	2.699	0.990
		298	5.762	2.689	1.036	0.956
		308	3.561	6.626	1.560	0.927
	BCP550	288	1.009	6.165	1.886	0.949
		298	1.091	44.168	2.751	0.989
		308	2.316	0.710	0.759	0.945
	FTBCP250	288	3.760	2.259	1.225	0.994
		298	4.247	7.673	1.225	0.917
		308	3.710	5.418	1.358	0.998
	FTBCP550	288	1.250	2.643	1.624	0.980
		298	1.197	8.782	1.779	0.946
		308	1.245	3.649	1.594	0.980
30 mg/L	BCP250	288	2.046	2.563	1.666	0.984
		298	2.724	22.907	2.411	0.968
		308	5.064	2.778	1.278	0.983
	BCP550	288	1.411	4.811	2.346	0.962
		298	1.389	18.930	3.329	0.912
		308	1.716	6.894	2.003	0.973
	FTBCP250	288	2.255	2.581	1.570	0.974
		298	3.183	3.589	1.609	0.982
		308	3.472	12.697	2.034	0.979
	FTBCP550	288	1.421	5.657	2.298	0.931
		298	1.640	12.418	1.551	0.950
		308	2.000	10.062	1.573	0.989

Table S5. Thermodynamic parameters calculated from different K values

DOMs	Carbon surface	Kc based				KL based				KF based			
		T (K)	ΔG (kJ/mol)	ΔH (kJ/mol)	ΔS (kJ/mol)	T (K)	ΔG (kJ/mol)	ΔH (kJ/mol)	ΔS (kJ/mol)	T (K)	ΔG (kJ/mol)	ΔH (kJ/mol)	ΔS (kJ/mol)
No HAs	BCP250	288	-7.532	-24.568	-0.058	288	-3.158	-64.018	-0.211	288	-6.322	-10.616	-0.015
		298	-7.012			298	-1.189			298	-5.661		
		308	-6.656			308	1.072			308	-6.036		
	BCP550	288	-3.454	-48.005	-0.150	288	1.808	-12.064	-0.042	288	-3.311	-47.373	-0.155
		298	-2.016			298	-0.604			298	-2.078		
		308	-0.773			308	2.839			308	-0.244		
	FTBCP250	288	-8.320	-23.196	-0.050	288	-4.065	-50.266	-0.160	288	-6.086	-13.544	-0.025
		298	-7.909			298	-1.845			298	-6.351		
		308	-7.164			308	-0.871			308	-5.555		
	FTBCP550	288	-5.466	-41.113	-0.116	288	-3.013	-16.428	-0.047	288	-3.265	-33.886	-0.106
		298	-4.899			298	-2.286			298	-2.966		
		308	-2.975			308	-2.087			308	-1.121		
10 mg/L HAs	BCP250	288	-3.224	31.419	0.116	288	0.641	11.956	0.041	288	-2.212	22.669	0.088
		298	-5.985			298	-0.905			298	-4.716		
		308	-4.732			308	-0.118			308	-3.902		
	BCP550	288	-0.300	10.077	0.038	288	0.458	27.187	0.093	288	0.182	2.035	0.007
		298	-2.030			298	-0.890			298	-0.623		
		308	-1.258			308	-1.389			308	0.070		
	FTBCP250	288	-3.687	16.545	0.072	288	0.455	14.550	0.052	288	-2.777	16.261	0.068
		298	-6.750			298	-2.569			298	-4.713		
		308	-5.056			308	-0.465			308	-4.069		
	FTBCP550	288	-0.316	8.572	0.040	288	1.401	20.760	0.070	288	0.228	3.990	0.014
		298	-1.620			298	-1.445			298	-0.322		
		308	-0.891			308	0.107			308	-0.023		
30 mg/L HAs	BCP250	288	-1.411	49.294	0.177	288	0.864	12.371	0.041	288	-0.845	43.141	0.153
		298	-3.930			298	-0.320			298	-2.890		
		308	-4.523			308	0.083			308	-3.887		
	BCP550	288	-0.506	21.758	0.078	288	0.882	20.037	0.067	288	-1.409	-8.296	-0.025
		298	-1.432			298	-0.404			298	-0.497		
		308	-1.954			308	-0.435			308	-0.946		
	FTBCP250	288	-1.710	31.252	0.116	288	1.168	12.105	0.038	288	-1.148	35.034	0.126
		298	-3.048			298	0.817			298	-2.414		
		308	-4.551			308	0.407			308	-3.660		
	FTBCP550	288	-0.785	43.931	0.156	288	0.174	46.916	0.165	288	-0.388	17.432	0.062
		298	-1.748			298	-3.949			298	-1.052		
		308	-3.175			308	-3.014			308	-1.625		

Table S6. Site energy distribution under different DOMs conditions.

NOMs	Carbon surface	Temperature (K)	n*	Cs (mg/L)	b* (L/mg)	μE* (KJ/mol)	σE* (KJ/mol)
No NOMs	BCP250	288	1.817	4.040	4.248	5.274	2.322
		298	2.435	4.160	3.774	4.892	1.819
		308	2.724	4.225	3.845	4.961	1.688
	BCP550	288	2.100	4.040	6.504	5.487	2.038
		298	1.993	4.160	2.274	4.585	2.172
		308	3.359	4.225	1.265	3.874	1.366
	FTBCP250	288	1.468	4.040	4.699	5.911	2.844
		298	1.513	4.160	5.242	6.280	2.873
		308	1.295	4.225	6.060	7.303	3.455
	FTBCP550	288	1.566	4.040	3.145	5.149	2.641
		298	2.491	4.160	2.599	4.493	1.770
		308	1.861	4.225	1.684	4.462	2.364
10 mg/L	BCP250	288	2.699	8.010	1.813	5.512	1.602
		298	1.036	10.430	5.762	10.034	4.232
		308	1.560	20.650	3.561	9.842	2.961
	BCP550	288	1.886	8.010	1.009	5.018	2.235
		298	2.751	10.430	1.091	5.889	1.628
		308	0.759	20.650	2.316	10.730	5.781
	FTBCP250	288	1.225	8.010	3.760	7.611	3.435
		298	1.225	10.430	4.247	8.761	3.589
		308	1.358	20.650	3.710	10.234	3.391
	FTBCP550	288	1.624	8.010	1.250	5.351	2.571
		298	1.779	10.430	1.197	6.077	2.473
		308	1.594	20.650	1.245	8.115	2.879
30 mg/L	BCP250	288	1.666	8.010	2.046	6.033	2.543
		298	2.411	20.430	2.724	8.505	1.862
		308	1.278	27.650	5.064	11.757	3.613
	BCP550	288	2.346	8.010	1.411	5.339	1.832
		298	3.329	20.430	1.389	7.719	1.350
		308	2.003	27.650	1.716	9.192	2.314
	FTBCP250	288	1.570	8.010	2.255	6.248	2.693
		298	1.609	20.430	3.183	9.261	2.778
		308	2.034	27.650	3.472	10.068	2.281
	FTBCP550	288	2.298	8.010	1.421	5.354	1.869
		298	1.551	20.430	1.640	8.274	2.866
		308	1.573	27.650	2.000	9.633	2.936

Reference

(1) Peak, D.; Ford, R. G.; Sparks, D. L. An in Situ ATR-FTIR Investigation of Sulfate Bonding Mechanisms on Goethite. *J. Colloid Interface Sci.* **1999,** *218* (1), 289-299.
(2) Miraboutalebi, S. M.; Nikouzad, S. K.; Peydayesh, M.; Allahgholi, N.; Vafajoo, L.; McKay, G. Methylene blue adsorption via maize silk powder: Kinetic, equilibrium, thermodynamic studies and residual error analysis. *Process Saf. Environ. Prot.* **2017,** *106*, 191-202.
(3) Sewu, D. D.; Boakye, P.; Woo, S. H. Highly efficient adsorption of cationic dye by biochar produced with Korean cabbage waste. *Bioresour. Technol.* **2017,** *224*, 206-213.
(4) Wang, P.; Cao, M.; Wang, C.; Ao, Y.; Hou, J.; Qian, J. Kinetics and thermodynamics of adsorption of methylene blue by a magnetic graphene-carbon nanotube composite. *Appl. Surf. Sci.* **2014,** *290*, 116-124.
(5) Senthilkumaar, S.; Kalaamani, P.; Porkodi, K.; Varadarajan, P. R.; Subburaam, C. V. Adsorption of dissolved Reactive red dye from aqueous phase onto activated carbon prepared from agricultural waste. *Bioresour. Technol.* **2006,** *97* (14), 1618-1625.
(6) Oke, I. A.; Olarinoye, N. O.; Adewusi, S. R. A. Adsorption kinetics for arsenic removal from aqueous solutions by untreated powdered eggshell. *Adsorption* **2008,** *14* (1), 73-83.
(7) Zhu, J.; Pigna, M.; Cozzolino, V.; Caporale, A. G.; Violante, A. Sorption of arsenite and arsenate on ferrihydrite: Effect of organic and inorganic ligands. *J. Hazard. Mater.* **2011,** *189* (1), 564-571.
(8) Konicki, W.; Aleksandrzak, M.; Moszyński, D.; Mijowska, E. Adsorption of anionic azo-dyes from aqueous solutions onto graphene oxide: Equilibrium, kinetic and thermodynamic studies. *J. Colloid Interface Sci.* **2017,** *496*, 188-200.